ELSEVIER

Journal of Marine Systems 35 (2002) 183–205

JOURNAL OF MARINE SYSTEMS

www.elsevier.com/locate/jmarsys

The effects of episodic rainfall events to the dynamics of coastal marine ecosystems: applications to a semi-enclosed gulf in the Mediterranean Sea

G. Arhonditsis*,[1], G. Tsirtsis, M. Karydis

Department of Marine Sciences, University of the Aegean, Sapfous 5, 81100 Mytilene, Greece

Received 11 January 2001; accepted 15 January 2002

Abstract

A modelling procedure of hourly time discretisation is developed in order to study the effects of episodic rainfall events to the dynamics of coastal marine environments. This methodology was applied on the gulf of Gera, Island of Lesvos, Greece, a semi-enclosed and shallow ecosystem surrounded by an intensively cultivated watershed. The simulation of biological and chemical processes in the water column was focused on the interactions of inorganic nutrients, primary producers and organic matter. The hydrodynamic behaviour of the area was estimated by the combination of the Princeton Ocean Model and a multiple-box mass balance approach in order to describe the tidal hydraulic regime. The estimation of nutrient fluxes due to non-point sources was based on a modification of the unit-mass response functions. The results have shown that nutrient loading from agricultural runoff could be considerable after episodic rainfall events, resulting in an increase of the nutrient stock from 40% to 60%. The responses of the primary producers are regulated from weather conditions of the following period and the residence time of excessive nutrient loads within the gulf that ranges from a time span of less than 10 days to 1 month period. The good fit between simulated and experimental data supports the view that this integrated modelling approach should be considered as a realistic reproduction of the dynamics of coastal marine ecosystems and be used for testing various scenarios concerning their sustainability.

Keywords: Marine eutrophication; Nutrient enrichment; Non-point pollution; Mediterranean Sea; Coastal zone; Mathematical model

1. Introduction

Shallow coastal lagoons and gulfs are a major type of land-margin ecosystems where ecological, biogeochemical and physical processes govern their response to nutrient enrichment and the extent to which they act as a ''filter'' for terrestrial inputs (Nichols and Boon, 1994). The difficulties and inaccuracies concerning the transport processes of nutrients through these systems were surpassed by the use of mathematical models. Individual components of basins in combination with the subsequent marine ecosystems have been modelled with varying levels of success to attempt to understand the inter-disciplinary nature of processes operating at the watershed or at the receiving seawater body (Spaulding, 1994). These models can be classified according to their level of sophistication and

* Corresponding author. Present address: Department of Civil and Environmental Engineering, University of Washington, 313B More Hall, Box 352700, Seattle, WA, USA. Tel.: +1-206-616-9145; fax: +1-206-685-9185.

E-mail addresses: georgea@u.washington.edu, garh@env.aegean.gr (G. Arhonditsis).

[1] Tel.: +30-251-36800; fax: +30-251-36809.

0924-7963/02/$ - see front matter
PII: S0924-7963(02)00081-7

potential field of application and each class is efficient for a range of simulations, which in principle cover any level of detail the user might deem necessary (Bouraoui and Dillaha, 1996).

A widespread simplified procedure presumes that inlet-basin systems oscillate in a pumping or Helmholtz mode; numerous of authors have solved the inlet momentum and basin continuity equations based on this consideration and a wide variety of other assumptions (Spaulding, 1994). The most thorough approach developed by Ozsoy (1977) reproduces successfully the behaviour of inlet-basin systems. This model is valid for the entire amplitude and frequency range and incorporates both friction and inertial terms. However, there is no spatial resolution for the transport processes inside the gulf and furthermore it has a disputable sensitivity in short time scales. The alternative methodology is the application of numerical methods such as the finite difference and finite element techniques (Isaji et al., 1985). Through careful selection of grid size, time step, calibration and validation with observational data these models can provide accurate predictions of flow and water quality, but they are computationally intensive (Spaulding, 1994). Moreover, the majority of cases presume conservative pollutants in order to obtain analytical solutions; an assumption that disables the understanding of microbial processes and nutrient cycling in the marine ecosystem (Visser and Kamp-Nielsen, 1996; Lesack et al., 1998).

In the present work, in view of the features of the aforementioned models, a modelling procedure has been developed in order to quantify the effects of episodic rainfall events to the dynamics of semi-enclosed marine environments. The model was evaluated in a Greek gulf, typical of the Mediterranean region, surrounded by a cultivated and inhabited watershed. This modelling effort consists of three interacting components which are the terrestrial, the hydrodynamic and the biological submodels. Special emphasis was placed on linking terrestrial and marine processes using hourly scale and appropriate spatial resolution, with a view of detecting accurately non-point nutrient loads and study their fate from the time they are imported into the gulf until they supply the primary producers or be flushed into the open sea. Furthermore, an alternative scenario concerning weather conditions was attempted in order to test the functioning and the carrying capacity of the ecosystem.

2. Methodology

2.1. The study area

The calibration and validation of the model was conducted within the gulf of Gera, Island of Lesvos, Greece, a semi-enclosed marine ecosystem with a mean depth of 10 m and a total volume of 0.9×10^9 m^3 (Fig. 1). The study watershed, a 194.01-km^2 drainage area, is intensively cultivated mainly with olive trees whereas the mountainous zones of the catchment are covered with evergreen sclerophyllous plant communities (maquis), phrygana in combination with coniferous trees, the so-called Mediterranean-type forest (Arhonditsis et al., 2000b). The livestock of the area numbers about 5500 sheep and goats; the animal husbandry is mostly of the domestic type, while free grazing is kept at low levels. Most of the local rivers, the main vectors of agricultural runoff and non-point nutrient loads are characterised by a torrential regime considerably influenced of local precipitation characteristics (intensity, duration, frequency of occurrence and antecedent precipitation). The annual rainfall ranges between 600 and 800 mm and usually two or three times a year extreme rainfall events take place accompanied by significant non-point nutrient fluxes especially from the northern and western part of the watershed, where the two most important torrents of the area are located. The dynamic behaviour of the seawater body after such episodic meteorological events is regulated by the hydrodynamic regime of the gulf, including the exchanges with the open sea, in combination with weather conditions of the following days such as light intensity and temperature. The simulation of these processes, resulting sometimes in serious phytoplanktonic blooms and sometimes in a temporary increase of nutrient concentrations without major consequences in the primary production of the marine ecosystem, constitutes the main aim of the present paper. Furthermore, the point discharges, such as sewerage from the 7000 inhabitants and wastewater from industrial activities, should be considered as another significant exogenous source of nutrients. The study of the seawater quality was based on the

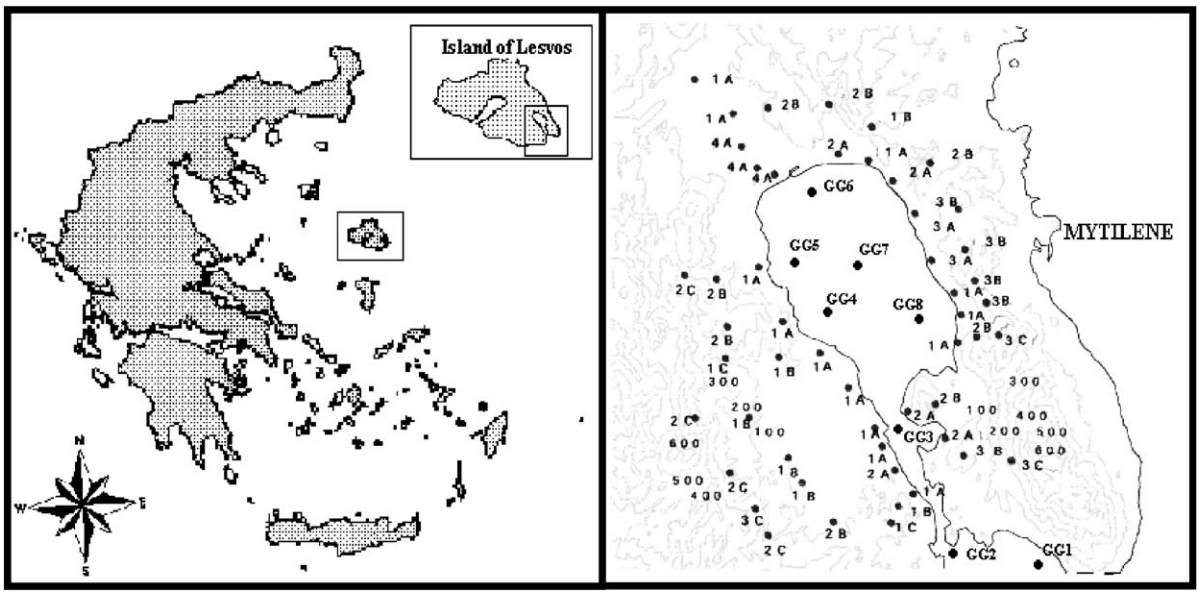

Fig. 1. The study area, the gulf of Gera, Island of Lesvos, Greece. The sampling sites of the marine (GG1–GG8) and the terrestrial ecosystem. (Land cover categories are: 1, cultivated olive groves; 2, abandoned olive groves; 3, maquis; and 4, wetlands. Letters A, B, and C correspond to the altitudes of <150, 150–300 and >300 m, respectively.)

information collected from eight sampling stations GG1–GG8 that are shown in Fig. 1. The experimental and analytical procedure and further details involving the physical, chemical and biological properties of the seawater body are reported elsewhere (Arhonditsis et al., 2000a).

2.2. The concept of the model

The quantification of the effects of episodic rainfall events to the dynamics of semi-enclosed marine environments was attempted using an integrated modelling approach that had an analogous structure with a former development (Arhonditsis et al., 2000a). It consisted of the same three interacting components, the terrestrial, the hydrodynamic and the biological submodels, but with modified or alternative formulas from the former edition that tented to enhance spatial and temporal resolution. The flow diagram of the model is shown in Fig. 2. The non-point fluxes of nutrients were estimated on hourly basis by a modification of the unit-mass response function (Rinaldo and Marani, 1987). Moreover, the assessment of the nutrient loads from atmosphere and point sources was obtained using empirical formulations and experimental data from the bibliography (see the following section). The hydrodynamic submodel was a kind of hybrid construction decomposing current speeds into tidal and non-tidal constituents. This model coupled the two-dimensional, vertically averaged mode of the Princeton Ocean Model (Mellor and Yamada, 1982), with the one-dimensional propagation of the tidal pulses. The two components of the hydrodynamic submodel were applied to the same grid-domain, but with the basic assumption that the seawater exchanges among the cells due to tidal forcing occurred in the latitudinal scale, whereas non-tidal transport caused both lateral and latitudinal flows. The third component was the biological submodel, focusing on the flow energy through the microbial components of marine food web (Tsirtsis, 1995). The spatial scale of this submodel coincided with the cells of the hydrodynamic grid-domain, where the equation of mass conservation was reduced by spatial averaging to a two-dimensional relation (Shanahan and Harleman, 1984). This 2-D perception of the system was supported by the experimental procedure and the statistical analysis of the data that revealed the vertical homogeneity of the seawater column (Arhonditsis et al., 2000a). Finally, the open sea, related with the oligotrophic

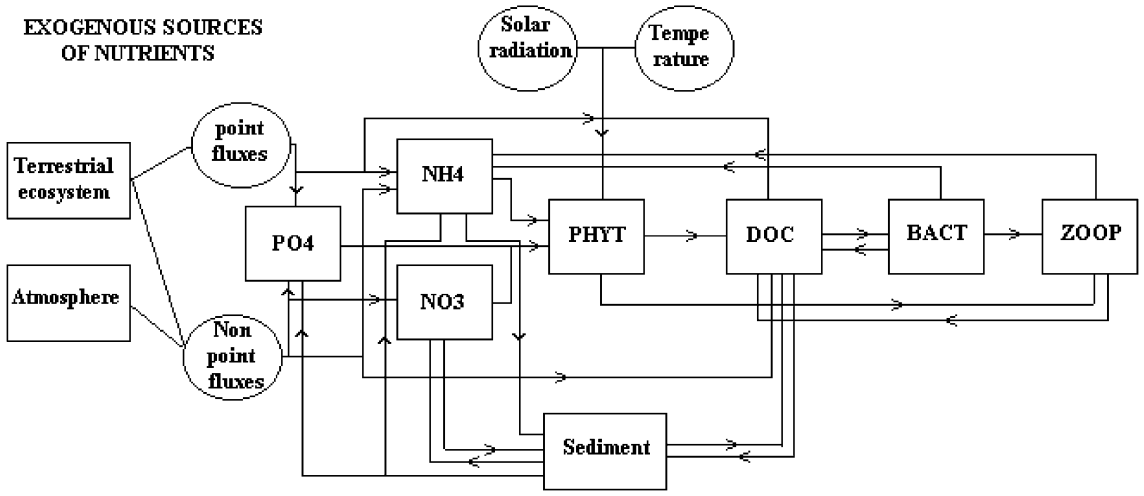

Fig. 2. Flow diagram of the biological submodel (PHYT, BACT and ZOOP are phytoplanktonic, bacterial and zooplanktonic biomasses, respectively).

waters of the Aegean Sea, has been used for defining boundary conditions.

The model calibration and validation were based on two independent data sets collected from the previous mentioned experimental work. The calibration of the model was obtained by a data set of twelve sampling cruises, involving the annual variation of the state variables over the gulf. On the other hand, the model validation was focused on the effects of single rainfall events to the dynamics of the subsequent water body, comparing predicted and observed values of marine state variables after the occurrence of six storm events.

3. The development of the simulation model

3.1. The terrestrial submodel

3.1.1. Nonpoint exogenous sources of nutrients

The model that was used for evaluating non-point nutrient loading from the terrestrial ecosystem is a modification of the modelling approach suggested by Rinaldo and Marani (1987). The agricultural land surrounding the water body was divided into unit source areas using a grid of 0.25×0.25 km. It was assumed that the unit areas are hydrologically active and the discrimination of their characteristics such as soil, crop, management and topographic properties was supported using GIS (Arc/Info, Environmental System Research Institute). The fundamental model structure may be described as the combination of a water quality component, based on a simple mass balance, with the Nash conceptual hydrologic model of rainfall–runoff transformations. The later component models the watershed as a cascade of continuously stirred tank reactors. According to this concept, the transfer function of a hydrologically active unit area to rainfall events distributed in time according to $i(\tau)$ is built by convolution as (Novotny and Chesters, 1981)

$$Q(t;n;k) = \int_0^t h(t-\tau;n;k)i(\tau)\mathrm{d}\tau$$

$$\text{where } h(t;n;k) = \frac{1}{k \cdot \Gamma(n)}(t/k)^{n-1}e^{-t/k}$$

where $Q(t;n;k)$ is the flow output (m^3/h) per unit source area (m^2), $h(t;n;k)$ is the ordinate of the instantaneous unit hydrograph (h^{-1}), τ is the lag time that corresponds to the time interval between maximum rain excess and the peak of the runoff (h), $i(\tau)$ is the impulse hyetograph (m/h), n is a dimensionless watershed characteristic representing approximately the number of reservoirs, $\Gamma(n)$ is the Gamma function of n and k is a storage constant (h^{-1}) related to the time of travel of rainwater from the most remote point on the watershed to the watershed outlet, the so-called

time of equilibrium or time of concentration t_e, by the expression $k = t_e/n$.

Furthermore, the conceptual scheme for the chemical mass transfer, in a continuously stirred tank reactor, is ruled by

$$\frac{\partial c}{\partial t} = h(c_e - c)$$

where c is the current nutrient concentration (mg/l) in the runoff volume (mobile phase), c_e is the equilibrium concentrations (mg/l) in the dissolved-phase (an interphase where solid or fixed and mobile phase are in equilibrium) and h is a mass transfer coefficient (h^{-1}) that measures the actual speed of chemical transfer from the interphase to the bulk of the runoff (Zingales et al., 1984). In the case where c_e is a time-independent variable and h is a spatial and temporal constant, the flow rate q of a nutrient and the total quantity Z in the watershed outlet are given by the following unit-mass response functions

$$q(t;n;k;h;c'_e) = c'_e \left\{ Q(t;n;k) - \left(\frac{k}{k+h}\right)^n Q(t;n;k+h) \right\}$$

$$Z(t;n;k;h;c'_e) = \int_0^t q(t;n;k;h;c'_e)\,dt = c'_e \left\{ V(t;n;k) - \left(\frac{k}{k+h}\right)^n V(t;n;k+h) \right\}$$

$$c'_e = \int_{y_1}^{y_2} \int_{x_1}^{x_2} c_e(x,y)\,dx\,dy$$

where $q(t;n;k;h;c'_e)$ is the nutrient flow rate (mg/h), $Z(t;n;k;h;c'_e)$ is the total nutrient load (mg) at time t, $Q(t;n;k)$ is the flow output (m^3/h) and $V(t;n;k)$ is the runoff volume discharge (m^3) at time t per unit area (m^2). Finally, the term c'_e constitutes an innovation of the present study, referring to the spatial variability of c_e over the basin. It is computed by integrating the function $c_e(x,y)$ over the catchment area, where x_1, x_2, y_1 and y_2 correspond to the coordinates of the watershed boundaries. The nutrient concentrations were determined by a dense sampling network that covered the entire watershed (Fig. 1); whereas the estimation of the solid and dissolved phase fraction was obtained through Langmuir (for phosphates) and Freundlich (for ammonium) isotherms (Arhonditsis et al., in press). Furthermore, the nitrates were assumed to be totally dissolved in soil moisture. The spatial distribution $c_e(x,y)$, was obtained by interpolating with the Inverse Distance-Weighting Method (Watson and Philip, 1985).

The calibration of the various parameters of the terrestrial model was obtained by systematic samplings on hourly basis during the occurrence of several rainfall–runoff events. Samples were taken from the outlets of the two basic torrents of the area, located on the northern and western part of the watershed. The field and analytical work involving the measured physical and chemical parameters of non-point discharges, in combination with theoretical aspects of the model and calibration results, has been described elsewhere (Arhonditsis et al., in press). Nutrient fluxes through atmospheric wet and dry depositions were also considered, based on local data and existing literature for the north-eastern Mediterranean (Herut and Krom, 1996; Medinets, 1996; Herut et al., 1999).

3.1.2. Exogenous point sources of nutrients and organic carbon

The most important point discharges in the water body under consideration are the domestic effluents and wastewater from the local industrial activities. This wastewater is mainly a by-product of the elaboration of oil crops by 'centrifugal' type oil presses and it can be characterised as 'plant' extract containing minor quantities of inorganic nitrogen and 0.03–0.05% of inorganic phosphorus (Michelakis and Koutsaftakis, 1989). The estimation of the nutrient loads from domestic effluents was based on available data for the human population of the area and bibliographic information. The total human population in the area surrounding the gulf of Gera is estimated to be 7064 people according to the 1991 census. Each year during the summer (especially in July and August), the whole area hosts approximately 5000 tourists, resulting in an increase of point loading of up to 35%. On the basis of the existing literature (Smith, 1977; Marchetti and Verna, 1992; Werner and Wodsak, 1994), it was assumed that the per capita contribution of inorganic nitrogen is 6.5 g/person day and of inorganic phosphorus is 2 g/person day, whereas the per capita contribu-

tions of the organic forms of these elements are 3.5 and 1 g/person day, respectively. The apportionment of the daily discharges in the hourly scale was obtained by taking into account the local habits and practices in combination with in situ measurements. Therefore, peak flows were assumed to occur during the midday, whereas the point loads in the night were approaching zero (Arhonditsis, 1998).

The terrestrial submodel was run with a time step of 1 h and the nutrient and organic carbon loads of the marine ecosystem were estimated on hourly basis. These loads were used as input for the biological submodel describing the flow of energy through microbial components of the marine ecosystem.

3.2. The hydrodynamic submodel

The simulation of the hydrodynamic regime of the gulf was obtained by separating tidal and non-tidal transport. The non-tidal circulation pattern including both barotropic (wind driven slopes of the water levels) and baroclinic forcing (salinity or temperature gradients) was based on the application of the Princeton Ocean Model (Mellor and Yamada, 1982). This free surface model has a sigma coordinate system in that the vertical axis is scaled on the water column depth, a necessary attribute in dealing with significant topographical variability such as that encountered in estuaries or over continental shelf breaks and slopes (Mellor, 1996). The 2-D mode of the model was deemed sufficient due to the exposed resemblance between the circulation pattern of the upper layer and that of the bottom (Arhonditsis et al., 2000a). In the present work, a rectangular grid was used with cell dimensions of 330×330 m and the wind stresses were incorporated using the Wilson's equation (Weiyan, 1992). The initial field for temperature and salinity was taken from the available observations collected from the sampling sites represented in Fig. 1. The model was run with a time step of 1 h, forced with the prevailing wind patterns of the time period under study, in order to simulate the 2-D hydrodynamic circulation.

The description of the tidal currents resulted from a detailed harmonic analysis of 30-year time series data of the area. The resultant tide is expressed as the sum of a number of simple harmonic (sine or cosine wave) constituents, each of which has its own characteristic period, phase and amplitude. The degree of distortion or asymmetry in the tidal waveform varies as the ratio of the constituent amplitudes, while the form of distortion is governed by the phase differences. The analysed constituents used for the study area are given in Table 1, which are considered sufficient to predict the tide to within about 5% (Pond and Pickard, 1983). Furthermore, it was assumed that the propagation of the tidal pulses for the inlet-gulf system could be simulated by progressive waves. Each tide component generates a separate oscillation that is transmitted inside the water body in one-dimensional mode creating a uniform front wave. The vertical displacement n of the free surface from the mean sea level (depth) is given in terms of time t (h) and horizontal displacement y (m), as the following sum of eight trigonometric equations of the form

$$n_y = \sum_{i=1}^{8} A_i \cos\left[2\pi\left(\frac{y}{L} - \frac{t}{T_i} - \Phi_i\right)\right]$$

where A, π and T are the amplitude (m), phase (°) and period (h) of a tidal constituent, L is the wavelength (m), which is perceived, for all the analysed constit-

Table 1
Characteristics of the analysed force constituents used for the prediction of tide in the study area

Species and name	Amplitude (m)	Period (solar hours)	Phase (°)
Semi-diurnal			
Principal lunar (M_2)	0.07	12.42	0
Principal solar (S_2)	0.03	12.00	23
Larger lunar elliptic (N_2)	0.01	12.66	− 12
Luni-solar semi-diurnal (K_2)	0.01	11.97	45
Diurnal			
Luni-solar diurnal (K_1)	0.04	23.93	64
Principal lunar diurnal (O_1)	0.03	25.82	18
Principal solar diurnal (P_1)	0.01	24.07	125
Long-period			
Lunar fortnightly (M_f)	0.01	327.9	− 31

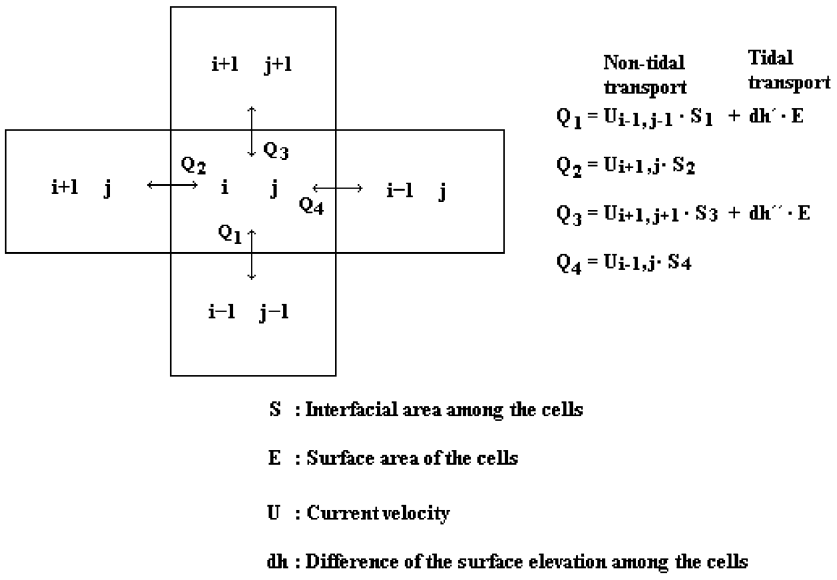

Fig. 3. Flow exchanges among an elementary volume *i*, *j* and its adjacent grid-cells, due to tidal and non-tidal transport (current velocity *U* is the resultant of the two nodal constituents of the interfacial areas among the cells).

uents of the tide, equal to the *Y* dimension (south to north) of POM's grid domain. The multiple-box character of the present model presumes that the seawater level is a discrete function of space. It was considered therefore that the tidal heights of the volume elements (the grid cells of POM) at time *t* are the elevations of their respective centroids, computed by the aforementioned method. Thus, the total volume exchanges among the grid cells are the sum of the 2-D non-tidal (*X* and *Y* axes) and the 1-D tidal (*Y*-axis) forcing components. The output of the hydrodynamic submodel was used for estimating mass transport for the biological submodel.

3.3. The biological submodel

The biological submodel was applied to the same rectangular grid with cell dimensions of 330 × 330 m, in order to increase spatial resolution and simulate accurately transport processes of the marine ecosystem. The experimental procedure revealed that nitrogen seems to be the limiting factor for primary production in the study area. However, both nitrogen and phosphorus have been considered to necessitate for the phytoplanktonic growth in order to test and generalise the applicability of the model. Furthermore, the partitioning of the nitrogen stock into nitrate and ammonium fractions enabled the distinction between the "new" and the "regenerated" primary production, respectively. The oligotrophic waters of the Aegean Sea, influencing the internal part of the gulf by mixing processes, have been used to define boundary conditions. It was assumed that the annual concentrations of nitrate, ammonium, phosphate, DOC, phytoplankton, bacteria and zooplankton in the open sea vary sinusoidally with time in good accordance with the experimental data (Arhonditsis et al., 2000a).

Therefore, it was considered that the simplest model that could be developed to describe energy flow through the microbial food web consists of seven state variables, phytoplanktonic (PHYT), zooplanktonic (ZOOP) and bacterial (BACT) biomasses, nitrate (NO_3), ammonium (NH_4), phosphate (PO_4) and dissolved organic carbon (DOC) concentrations (Fig. 3). The seven differential equations describing the temporal variations of the state variables are

$$\mathrm{dPHYT}/\mathrm{d}t = (\mu(1-\gamma) - m_\mathrm{p} - k_\mathrm{WS})\mathrm{PHYT} - G_p \pm \mathrm{PHYT}_\mathrm{comp}$$

$$\mathrm{dBACT}/\mathrm{d}t = (U_1 + U_2 - m_\mathrm{b} - e_\mathrm{b} - k_\mathrm{WS})\mathrm{BACT} - G_\mathrm{b} \pm \mathrm{BACT}_\mathrm{comp}$$

$$\mathrm{dZOOP}/\mathrm{d}t = as_\mathrm{p}G_\mathrm{p} + as_\mathrm{b}G_\mathrm{b} - (e_\mathrm{z} + m_\mathrm{z})\mathrm{ZOOP} \pm \mathrm{ZOOP}_\mathrm{comp}$$

$$\mathrm{dDOC}/\mathrm{d}t = (\mu\gamma + m_\mathrm{dp})\mathrm{PHYT} + (m_\mathrm{db} - U_1)\mathrm{BACT} + (e_\mathrm{dz} + m_\mathrm{dz})\mathrm{ZOOP} + \mathrm{DOC}_\mathrm{sed} + \mathrm{DOC}_\mathrm{point} + \mathrm{DOC}_\mathrm{npoint} + \mathrm{DOC}_\mathrm{atm} \pm \mathrm{DOC}_\mathrm{comp}$$

$$\mathrm{dNH_4}/\mathrm{d}t = -(a_\mathrm{N}\mathrm{NH}_\mathrm{4UP}N_\mathrm{fb} - m_\mathrm{ap})\mathrm{PHYT} + (m_\mathrm{ab} + e_\mathrm{b} - U_2)\mathrm{BACT} + (e_\mathrm{az} + m_\mathrm{az}) \times \mathrm{ZOOP} + \mathrm{NH}_\mathrm{4sed} + \mathrm{NH}_\mathrm{4point} + \mathrm{NH}_\mathrm{4npoint} + \mathrm{NH}_\mathrm{4atm} \pm \mathrm{NH}_\mathrm{4comp}$$

$$\mathrm{dNO_3}/\mathrm{d}t = -a_\mathrm{N}\mathrm{NO}_\mathrm{3UP}N_\mathrm{fb}\mathrm{PHYT} + \mathrm{NO}_\mathrm{3sed} + \mathrm{NO}_\mathrm{3point} + \mathrm{NO}_\mathrm{3npoint} + \mathrm{NO}_\mathrm{3atm} \pm \mathrm{NO}_\mathrm{3comp}$$

$$\mathrm{dPO_4}/\mathrm{d}t = -(a_\mathrm{P}\mathrm{PO}_\mathrm{4UP}P_\mathrm{fb} - m_\mathrm{pp})\mathrm{PHYT} + \mathrm{PO}_\mathrm{4sed} + \mathrm{PO}_\mathrm{4point} + \mathrm{PO}_\mathrm{4npoint} + \mathrm{PO}_\mathrm{4atm} \pm \mathrm{PO}_\mathrm{4comp}$$

The transfer coefficients and the model parameters of the equations are described in Tables 4 and 5. The subscripts sed, point, npoint and atm indicate fluxes from the sediment, the point, non-point terrestrial sources and the atmosphere, respectively. The subscript comp indicates transport processes among the spatial compartments (cells) of the study area.

3.3.1. The physical forcing

Three physical factors were taken into account for the model construction: the temperature, the solar irradiance and the exchanges of chemical and biological parameters among the grid cells due to advective transport. The temperature was computed on hourly basis with the use of the Princeton Ocean Model. The diurnal variation of surface solar radiation was assumed to be represented by an isosceles triangle (Steele, 1962). The height of each daily triangle was the midday value and the base was equal to the respective photoperiod, whereas the light intensity for the night was 0. The annual variations of the photoperiod Φ_t (h) and the midday values of the surface solar radiation I_t (MJ/m^2 day) for a cloudless sky, were represented by the following equations

$$I_t = 12 - 5\cos\frac{2\pi t}{365}, \quad \Phi_t = 11.5 - 2.5\cos\frac{2\pi t}{365}$$

where t is the time (days) and the value 1 was assigned to the 1st of January. Furthermore, the model takes into account the decrease of light intensity due to cloudiness, with respect to the local meteorological data. Thus, the study distinguishes between three types of cloudiness associated with a decrease of the I_t values on a ratio of 25%, 50% and 75%. Given the assumption of the isosceles triangle, this decrease of the I_t values results in an equal decrease of the daily solar power (area of the triangle), which is distributed proportionally into the hours of the day (the lowering of the two equal sides of the triangle). However, this seems to be an inaccurate reproduction of reality because cloudiness and intensity of sunlight extinction have rarely uniform diurnal distribution, especially in the Mediterranean region. This perception may lead to minor discrepancies among experimental and simulated data in small time scales, but the deviations are smoothed during the night given the fact that computed and observed total solar irradiance per day are equal. The transport of chemical and biological parameters among the grid cells was estimated using the multiple-box model approach (Shanahan and Harleman, 1984). The exchanges among the spatial compartments due to diffusion were computed, from the former development, to be less than 1% in proportion to the advective motion (Arhonditsis et al., 2000a). Therefore, these microscale turbulent fluctuations, represented by a number of dispersion coefficients, were excluded from the simulation procedure in order to decrease computational demands. Thus, the concentrations of the state variables in each cell are determined by simple mass balance, essentially the integration of the equation of mass conservation over the volume element (cell). For an arbitrary configuration of elements, the differential equation for element k is

$$V_k\frac{\mathrm{d}c_k}{\mathrm{d}t} = \sum_j \left[Q_{jk}c_j - Q_{kj}c_k\right] + S_k$$

where c_k is the concentration in element k (μg-at/l or mg/m^3), V_k is the volume of element k (m^3), S_k is the sum of all sources and sinks within element k and Q_{jk} is the flow from element j to k (m^3/h) computed from the output of the hydrodynamic submodel by summing the flows between cells j and k, due to tidal (latitudinal direction) and non-tidal transport (latitudinal and longitudinal direction), as it is illustrated in Fig. 3.

3.3.2. Nutrient fluxes from the sediment

The nitrogen exchange at the seawater–sediment interface was estimated according to the empirical formulation of Jacobsen and Jorgensen (1975). Diffusion processes of the interstitial phosphorus from pore water to the seawater column were estimated by means of a modification of the Kamp-Nielsen (1975) approximation (valid at 7 °C) to account for larger ranges of temperature. The computed fluxes from these forms were incorporated into the respective differential equations based on the assumption that the nutrient release rate from the sediment is uniform during the day. Furthermore, the plankton exchanges between sediment and seawater are also incorporated in the model; they are expressed explicitly in the phytoplankton and bacterial equations by the parameter k_{WS}.

3.3.3. The phytoplankton equation

Phytoplanktonic growth depends on light and nutrient availability and on the temperature conditions. The phytoplanktonic growth rate μ can be written in general functional form as

$$\mu = \mu_{max}(T_{ref}) f(T) f(I) f(N,P)$$

where $\mu_{max}(T_{ref})$ is the maximum growth rate at a particular reference temperature (T_{ref}) under conditions of saturated light intensity and excess of nutrients (h^{-1}), $f(T)$ is the temperature function for growth, $f(I)$ and $f(N,P)$ are the growth limiting functions for light intensity and nutrients (nitrogen and phosphorus). The temperature function (Table 2a) was obtained by combining the two logistic equations developed by Coffaro and Bocci (1997). One equation accounts for temperatures lower than the optimum and the other for temperatures above the optimal. This set of formulations was developed primarily for species of magroalgae, but it was assumed that after an appropriate calibration would be sufficient to describe the mean influence of temperature on the entire phytoplanktonic community. The light limitation on phytoplanktonic growth (Table 2b) was expressed by the model proposed by Taylor and Joint (1990). The effects of nutrients to the algal growth (Table 2c) were based on the determination of the growth limitation factors as a function of the intracellular inorganic nitrogen and phosphorus concentrations at each time step (Davidson, 1996; Coffaro and Sfriso, 1997). Phytoplanktonic losses are assumed to be due to biological (exudation, mortality and zooplankton grazing) and physical factors (mixing processes caused by advection). The chlorophyll a content of the phytoplanktonic cells is converted to carbon assuming a C/chl$a$ ratio of 50 (Fasham et al., 1990).

Table 2
The phytoplankton growth limiting functions (a) for temperature, (b) light intensity and (c) nutrients (nitrogen and phosphorus)

(a) $f(T) = K_a(T)K_b(T)$ where

$K_a(T) = \frac{k_1 e^{(\gamma_1(T-T_{min}))}}{1+(k_1 e^{(\gamma_1(T-T_{min}))}-1)}$, $K_b(T) = \frac{k_2 e^{(\gamma_2(T_{max}-T))}}{1+(k_2 e^{(\gamma_2(T_{max}-T))}-1)}$ and

$\gamma_1 = \frac{1}{T_{opt}-T_{min}} \ln\left(\frac{0.98(1-k_1)}{k_1(1-0.98)}\right)$, $\gamma_2 = \frac{1}{T_{max}-T_{opt}} \ln\left(\frac{0.98(1-k_2)}{k_1(1-0.98)}\right)$

(b) $\varphi_{LT} = \ln\{(1+I/I_k)/[1+I\exp(-kz)/I_k]\}/(kz)$

$k = k_w + k_c C$

(c) $f(N,P) = \min\left\{1-\frac{N-N_{min}}{N_{max}-N_{min}}, 1-\frac{P-P_{min}}{P_{max}-P_{min}}\right\}$

$\frac{dN}{dt} = N_{up}N_{fb} - \mu\dot{N}$, $\frac{dP}{dt} = P_{up}P_{fb} - \mu\dot{P}$

$NH_{4UP} = VNH_{4max}\frac{NH_4}{NH_4+AH}$, $NO_{3UP} = VNO_{3max}\frac{NO_3\exp(-\phi NH_4)}{NO_3+NH}$

$PO_{4UP} = VPO_{4max}\frac{PO_4}{PO_4+PH}$

$N_{fb} = \frac{N_{max}-N}{N_{max}-N_{min}}$, $P_{fb} = \frac{P_{max}-P}{P_{max}-P_{min}}$

3.3.4. The bacterial equation

The model proposed by Fasham et al. (1990) has been used to describe bacterial growth. According to this model, the bacterial growth depends on the availability of dissolved organic nitrogenous compounds (DON) and ammonium. In a balanced growth situation, the ratio of bacterial ammonium uptake to DON uptake should be constant so as to ensure that bacterial biomass of the required C/N ratio is produced. This concept is incorporated into a Michaelis–Menten model of bacterial uptake by defining a total bacteria nitrogenous substrate S (Table 3). Bacterial

Table 3
The equations of (a) bacterial DON (U1) and ammonium (U2) uptake; (b) zooplankton grazing rates

(a)	$S = \min(NH_4, vDON)$
	$U_1 = \frac{a_{BD}DON}{DH+S+DON}$ and $U_2 = \frac{a_{BD}S}{DH+S+DON}$
(b)	$G_z = G_p + G_b$
	$G_z = gZOOP\frac{F}{K_z+F}$
	$F = p_1PHYT + p_2BACT$
	$p_1 = \frac{PHYT}{PHYT+BACT}$, $p_2 = \frac{BACT}{PHYT+BACT}$
	$G_p = gZOOP\frac{p_1PHYT}{K_z+F}$, $G_b = gZOOP\frac{p_2BACT}{K_z+F}$

losses are assumed to be due to exudation, mortality and zooplankton grazing. The bacterial biomass is calculated on the assumption of a carbon content of 20 fg/cell (Lee and Fuhrman, 1987).

3.3.5. The zooplankton equation

The model proposed by Fasham et al. (1990) has been used for the zooplanktonic growth. According to this model, the zooplanktonic growth is based on the selective grazing of phytoplankton and bacteria, which is controlled by the relative proportion of the two prey concentrations (Arhonditsis et al., 2000a). The mathematical formulations that simulate the zooplanktonic grazing rate are reported in Table 3. Losses of the zooplanktonic biomass are due to excretions and mortality including grazing by higher predators of the trophic chain. Moreover, these products of the zooplankton metabolism were assumed to constitute an indirect source of ammonium and dissolved organic carbon, in order to quantify their contribution to nutrient cycling (Table 4).

3.3.6. The ammonium equation

Ammonium is utilised by phytoplankton and bacteria as a source of nitrogen. Endogenous sources of ammonium are the planktonic exudation and the bacterial mineralisation processes, whereas exogenous fluxes result from domestic effluents, sediment and non-point sources.

3.3.7. The nitrate equation

The processes which have been considered were nitrate uptake by the phytoplankton, fluxes from the sediment and inflows from terrestrial sources.

3.3.8. The DOC equation

The major endogenous sources of DOC are phytoplanktonic, bacterial and zooplanktonic excretions and mortality, whereas the only biological sink is bacterial utilisation. The input of organic carbon from atmosphere, domestic effluents and industrial activity were also incorporated into the model. The dissolved organic carbon concentration is computed from the dissolved organic nitrogen data available, assuming a C/N ratio of 5.6 (Redfield et al., 1963).

3.3.9. The phosphate equation

The inorganic phosphorus stock of the seawater column is regulated by the fraction of the phytoplanktonic mortality that resupplies the seawater column, the phytoplanktonic uptake and the fluxes from sediment, atmosphere, point and non-point exogenous sources.

The set of ordinary differential equations defining the biological and chemical processes in the grid-cells of the biological submodel was integrated with a

Table 4
Description and definition of the transfer coefficients of the differential equations describing the temporal variation of the state variables in the biological submodel

Transfer coefficient	Description	Definition	Units
m_{dp}	Phytoplanktonic mortality to DOC	$m_p \times p4$	h^{-1}
m_{ap}	Phytoplanktonic mortality to ammonium	$m_p \times 0.071393 \times p5/p1$	h^{-1}
m_{pp}	Phytoplanktonic mortality to DIP	$m_p \times 0.032258 \times p14/p13$	h^{-1}
m_{db}	Bacterial mortality to DOC	$m_b \times p6$	h^{-1}
m_{ab}	Bacterial mortality to ammonium	$m_b \times 0.071393 \times p7/p2$	h^{-1}
m_{dz}	Zooplanktonic mortality to DOC	$m_z \times p8$	h^{-1}
m_{az}	Zooplanktonic mortality to ammonium	$m_z \times 0.071393 \times p9/p3$	h^{-1}
e_{dz}	Zooplanktonic excretions to DOC	$e_z \times p10$	h^{-1}
e_{az}	Zooplanktonic excretions to ammonium	$e_z \times 0.071393 \times p11/p3$	h^{-1}
a_N	Inorganic nitrogen to phytoplankton	$p12 \times 0.071393/p1$	dimensionless
a_P	Inorganic phosphorus to phytoplankton	$p12 \times 0.032258/p13$	dimensionless

fourth-order Runge-Kutta algorithm and a time step of 1 h. The simulation was run until initial conditions-independent patterns were achieved (5 years). The calibration of the model was focused on the cells that coincided with the sampling stations and took into consideration the respective experimental data. These values were smoothed by the use of a polynomial of degree 9 in order to isolate random errors of the experimental procedure and calibrate objectively the model with the "controlled random search" method. The output of the terrestrial submodel describing the nutrient and organic carbon exogenous loads and the output of the hydrodynamic submodel estimating the transport of nutrients and organic carbon due to the hydrodynamic circulation, both computed on an hourly basis, were used as inputs for the biological submodel.

4. Results and discussion

4.1. Results of the model

The model has shown good fit to the experimental data, since the main trends of the annual fluctuation of the state variables under consideration were predicted. The simulation was considered successful for phyto-planktonic and bacterial biomasses, nitrate and DOC concentrations, whereas minor discrepancies were observed for ammonium and phosphate. The temporal variability of the seven state variables of the model, in the spatial compartment that corresponds to the station GG3, is shown in Figs. 4 and 5. Similar inferences could be extracted from the rest elements of the grid. The presentation of this particular site was due to its complicated dynamics, since it is influenced by both exogenous point and non-point nutrient loading and interacts with the open sea. The parameter values obtained after the calibration are shown in Table 5. Moreover, the quantitative assessment of the goodness-of-fit between experimental and simulated data over the six internal stations was performed by the two-sided Kolmogorov–Smirnov test (Table 6), where in most cases the statistics indicate that the simulated values of the state variables do not vary significantly from those monitored in the marine ecosystem.

The model results indicated the circulation pattern of the area and the exchanges with the open sea as a

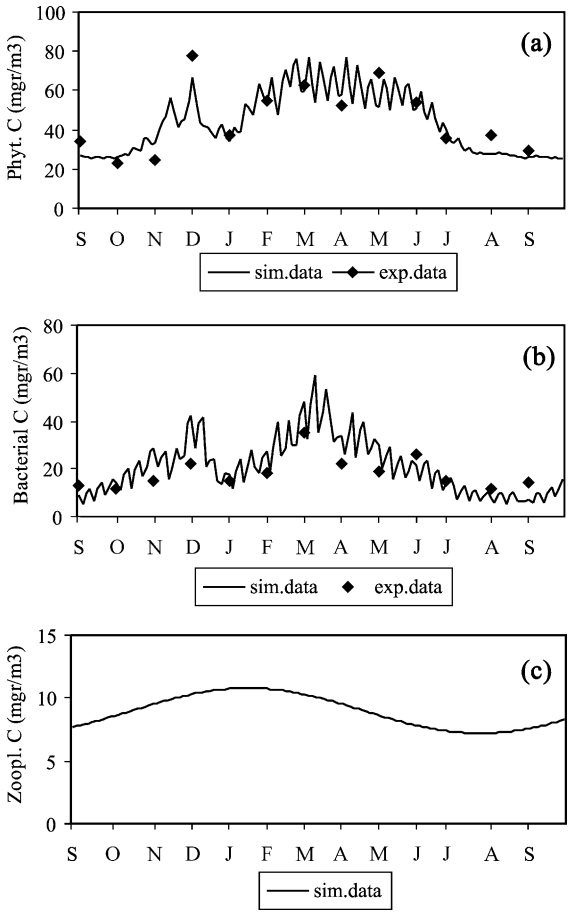

Fig. 4. Temporal variability of (a) phytoplanktonic, (b) bacterial and (c) zooplanktonic biomasses in the spatial compartment (grid-cell) that corresponds to the sampling station GG3 of the study area: simulated and experimental data.

significant factor for the functioning of the marine ecosystem. During the winter period, the ambient temperature and the inflows of the cold-water masses of the runoff constitute this shallow gulf denser than the external system. This regime in combination with the semi-enclosed character of the area limit the entrance of the oligotrophic waters of the Aegean Sea and the area exposes a cyclonic pattern with current velocities no larger than 0.02 m/s. Additionally, in the same period, the tidal motions do not play a major role neither in the values nor in the directions of the currents. Conversely, the warm months of the year (April–October), the limiting physical factors are eliminated and the gulf is characterised by an anticyclonic pattern with velocities

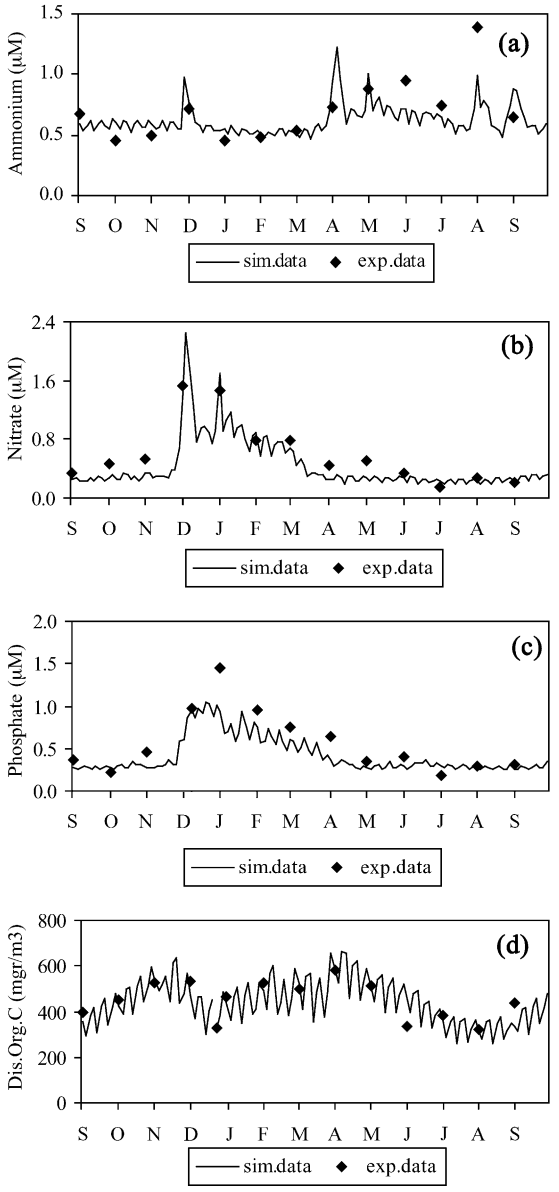

Fig. 5. Temporal variability of (a) nitrate, (b) ammonium, (c) phosphate and (d) dissolved organic carbon (DOC) concentrations in the spatial compartment (grid-cell) that corresponds to the sampling station GG3 of the study area: simulated and experimental data.

of 0.04–0.08 m/s. The tidal forcing accounts for 50–80% of the current speeds and distorts significantly their directions, especially during the spring tides. The experimental observations (expressing both tidal and non-tidal constituents) verified the qualitative and the quantitative results of POM, since the measured current velocities and directions during the winter period coincided with the simulated data. On the other hand, the summer values were at least twofold in comparison with the model outputs and were differing significantly in direction, possibly due to the tidal forcing that is computed separately.

The aforementioned annual fluctuations of the material exchanges between the gulf and the open sea can explain the temporal variability of the various chemical and biological state variables of the model. During the cold months of the year, when the gulf exhibits a degree of isolation, exogenous nutrients accumulate in the seawater body. Meanwhile, the physical factors (light intensity and temperature) have a limiting character; thus the autotrophic microorganisms do not consume a major fraction of the nutrient stock and the ecosystem is protected from serious phytoplanktonic blooms (<80 mg C/m^3). The predicted high levels of nutrient concentrations and the moderate responses of the primary production confirmed this conceptual scheme. This situation is reversed gradually until the summer, when significant inflows of the oligotrophic waters of the Aegean Sea seem to have a purification action. The excessive nutrient loads are flushed out of the gulf and the seawater can be renewed in a time span of ten days, especially under favourable combinations of the physical condition (spring tides and north winds). However, ammonium and organic carbon presented increasing trends in the same period, and this exceptional behaviour revealed that they are related mostly to autochthonous sources such as the biological activity (mortality, exudation). The zooplanktonic biomass has not shown considerable changes during the year and this was attributed to the fact that the phytoplanktonic and bacterial biomasses are enough to support the zooplanktonic growth, even when the prey populations were remarkably low (Arhonditsis et al., 2000a). Finally, the predicted nutrient concentrations exposed several peaks, resulting from event-based nutrient fluxes from the terrestrial ecosystem. These pulses were transmitted adequately in the rest trophic chain of the ecosystem. Therefore, it seems that the model exposes enhanced sensitivity for studying system dynamics in a scale of single precipitation events, which was another basic aim of its construction. This aspect of the model will be further analysed in a following paragraph.

Table 5
Description and values of the biological submodel parameters after the calibration of the model

Parameter	Description	Value	Units
γ	Fraction of phytoplanktonic production exudated as DOC	0.20	dimensionless
m_p	Phytoplanktonic mortality rate	0.014	h^{-1}
m_b	Bacterial mortality rate	0.036	h^{-1}
m_z	Zooplanktonic mortality rate	0.007	h^{-1}
k_{WS}	Exchange coefficient between sediment and seawater for phytoplankton and bacteria	0.095	h^{-1}
k_{SNO_3}	Rate constant for nitrate release from sediment	0.0042	$days^{-1}$
k_{SNH_3}	Rate constant for ammonium release from sediment	0.0038	$days^{-1}$
k_{SorgN}	Rate constant for organic nitrogen release from sediment	0.0040	$days^{-1}$
k_{SP}	Rate constant for inorganic phosphorus release from sediment	1.24	$days^{-1}$
NH	Half saturation constant for nitrate phytoplanktonic uptake	1.00	μg-at N/l
AH	Half saturation constant for ammonium phytoplanktonic uptake	1.00	μg-at N/l
PH	Half saturation constant for phosphate phytoplanktonic uptake	0.45	μg-at N/l
μ_{max}	Maximum specific growth rate for phytoplankton	0.138	h^{-1}
e_b	Bacterial excretion rate	0.004	h^{-1}
e_z	Zooplanktonic excretion rate	0.005	h^{-1}
as_p	Zooplanktonic assimilation efficiency of phytoplankton	0.75	dimensionless
as_b	Zooplanktonic assimilation efficiency of bacteria	0.75	dimensionless
DH	Half saturation constant for bacterial uptake	135	mg/m^3
I_k	Half saturation light intensity	2.50	MJ/m^2 h
K_w	Light extinction coefficient for water without chlorophyll	0.16	m^{-1}
K_c	Light extinction coefficient due to chlorophyll	0.19	$l\cdot(\mu g\cdot m)^{-1}$
k_1	Temperature adjustment coefficient	0.30	dimensionless
k_2	Temperature adjustment coefficient	0.01	dimensionless
T_{min}	Minimum temperature	25	°C
T_{max}	Maximum temperature	18	°C
T_{opt}	Optimum temperature	8	°C
N_{min}	Minimum internal quota for nitrogen	3.14	(μg-at N/mg dw)
N_{max}	Maximum internal quota for nitrogen	5.57	(μg-at N/mg dw)
P_{min}	Minimum internal quota for phosphorus	0.35	(μg-at P/mg dw)
P_{max}	Maximum internal quota for phosphorus	1.35	(μg-at P/mg dw)
VNH_{4max}	Maximum uptake rate for ammonium	0.75	(μg-at N/mg dw·h)
VNO_{3max}	Maximum uptake rate for nitrate	0.60	(μg-at N/mg dw·h)
VPO_{4max}	Maximum uptake rate for phosphorus	0.25	(μg-at P/mg dw·h)
ψ	Strength of the ammonium inhibition of nitrate uptake	0.60	$(\mu g\text{-at N/l})^{-1}$
v	Ratio of bacterial ammonium uptake to DON uptake	0.60	dimensionless
a_{BD}	Maximum bacterial uptake rate	0.156	h^{-1}
g	Zooplanktonic maximum specific growth rate	0.032	h^{-1}
K_Z	Half-saturation constant for zooplanktonic grazing	0.95	mg/m^3
p_1	C/N for phytoplankton	5.60	dimensionless
p_2	C/N for bacteria	4.50	dimensionless
p_3	C/N for zooplankton	6.00	dimensionless
p_4	Fraction of phytoplanktonic mortality becoming DOC	0.35	dimensionless
p_5	Fraction of phytoplanktonic mortality becoming ammonium	0.15	dimensionless
p_6	Fraction of bacterial mortality becoming DOC	0.35	dimensionless
p_7	Fraction of bacterial mortality becoming ammonium	0.15	dimensionless
p_8	Fraction of zooplanktonic mortality becoming DOC	0.30	dimensionless
p_9	Fraction of zooplanktonic mortality becoming ammonium	0.15	dimensionless
p_{10}	Fraction of zooplanktonic excretions becoming DOC	0.30	dimensionless
p_{11}	Fraction of zooplanktonic excretions becoming ammonium	0.15	dimensionless
p_{12}	Ratio of dry weight to organic carbon	2.50	dimensionless
p_{13}	C/P for phytoplankton	40.00	dimensionless
p_{14}	Fraction of phytoplanktonic mortality becoming DIP	0.17	dimensionless

Table 6
Model calibration: results of the two-Sided Kolmogorov–Smirnov goodness-of-fit test between experimental and simulated values of the state-variables, at the six internal stations of the gulf

State variables	Stations					
	GG3	GG4	GG5	GG6	GG7	GG8
Phytoplanktonic biomass	0.214[a]	0.315[a]	0.309[a]	0.158[a]	0.339[a]	0.135[a]
Bacterial biomass	0.418[a]	0.510	0.343[a]	0.259[a]	0.376 [a]	0.324[a]
Zooplanktonic biomass	0.381[a]	0.194[a]	0.389[a]	0.215[a]	0.316 [a]	0.191[a]
Nitrate concentration	0.214[a]	0.235[a]	0.334[a]	0.235[a]	0.224 [a]	0.257[a]
Ammonium concentration	0.296[a]	0.535	0.284[a]	0.463[a]	0.368[a]	0.518
Phosphate concentration	0.241[a]	0.467[a]	0.238[a]	0.295[a]	0.522	0.417[a]
DOC concentration	0.237[a]	0.199[a]	0.229[a]	0.203[a]	0.252[a]	0.256[a]

[a] Good accordance between simulated and experimental data at the 0.05 level of significance.

4.2. Results of the sensitivity analysis

The extent to which uncertainties in the values of parameters influence the equilibrium values of the state-variables was carried out by changing separately each model parameter and measuring the response of several state variables such as the maxima in phytoplanktonic, bacterial and zooplanktonic biomass. The sensitivity analysis was focused on the most uncertain parameters of the model that were estimated from the calibration procedure. Each model parameter was reduced at half and then increased twofold and the percentage changes of the maxima in phytoplanktonic, bacterial and zooplanktonic biomass were estimated by the model.

The results of the sensitivity analysis of the model are presented in Table 7. It was indicated that the model reacts with a remarkable stability to the uncertainties of the model parameters. The phytoplanktonic growth seems to be more liable to rapid changes. It depends mainly on the maximum phytoplanktonic specific growth rate (μ_{max}) and mortality (m_p), as well as on the fraction of phytoplanktonic production exudated as DOC (γ). The half saturation constant for bacterial uptake (DH), the maximum bacterial uptake rate (a_{BD}) and mortality rate (m_b) are the critical model parameters for bacterial biomass growth. Fi-

Table 7
Sensitivity evaluation for phytoplanktonic, bacterial and zooplanktonic biomass; percentage changes in phytoplanktonic, bacterial and zooplanktonic biomass maxima induced after the twofold increase and half reduction of the model parameters

Parameter	Sensitivity evaluation					
	Twofold increase			Half reduction		
	Phytoplanktonic biomass	Bacterial biomass	Zooplanktonic biomass	Phytoplanktonic biomass	Bacterial Biomass	Zooplanktonic biomass
γ	− 13.5	2.9	− 0.4	7.8	− 0.3	0.2
e_b	0.2	− 2.1	0.0	− 0.5	2.4	0.3
e_z	3.5	2.2	− 1.6	− 1.4	− 0.2	1.1
m_p	− 24.9	2.4	− 0.8	18.9	− 0.2	1.2
m_b	1.5	− 20.3	− 0.3	− 0.2	16.3	0.5
m_z	19.7	3.5	− 9.7	− 10.8	− 2.9	8.2
μ_{max}	29.3	− 0.2	0.5	− 21.2	3.9	− 1.3
a_{BD}	− 1.1	13.2	0.0	0.9	− 11.4	0.5
g	− 18.2	− 2.0	4.5	13.7	5.9	− 5.5
NH	− 5.5	0.1	− 0.2	5.2	− 0.2	0.8
AH	− 7.7	0.1	− 0.3	8.8	− 0.5	0.5
PH	− 6.2	0.3	− 0.4	9.3	− 0.7	0.6
DH	4.6	− 19.0	− 0.7	− 3.6	11.8	0.5
VNH_{4max}	11.2	− 2.2	0.5	− 11.8	2.2	− 1.2
VNO_{3max}	9.7	− 0.8	0.4	− 12.2	1.9	− 0.3
VPO_{4max}	14.5	− 0.4	0.5	− 17.9	1.4	− 1.5
I_k	− 4.9	2.5	− 0.5	9.8	− 0.3	0.7
K_Z	8.8	7.9	− 4.3	− 9.9	− 5.6	7.2

The notation is explained in Table 4.

nally, the zooplanktonic biomass is quite stable to the changes of the model parameters and it is related mostly to the mortality rate (m_z). Generally, these results are almost identical to those of the former development. Thus, in a similar way, it can be stated that the aggregated structure of the biotic compartments is efficient and credible to describe the function of the system with a view of interlinking terrestrial and marine processes (Arhonditsis et al., 2000a).

However, some parameters that are related to algal species and to their cell sizes such as the half saturation constants for nitrate (NH), ammonium (AH) and phosphorus (PH) phytoplanktonic uptake exposed a greater uncertainty than in the former model. Analogous evidences could be extracted from the remarkable sensitivities of the maximum uptake rates for ammonium (VNH_{4max}), nitrate (VNO_{3max}) and phosphorus (VPO_{4max}). Therefore, it seems possible that the adoption of the Caperon/Droop model to determine the effects of nutrients to algal growth increases the influences of the qualitative alterations of phytoplankton community (e.g. morphological characteristics, species composition) to the simulation results. A detailed structural analysis concerning the effects of the different formulations of the phytoplanktonic growth on the sensitivity of eutrophication models constitutes the aim of a current research.

4.3. Validation of the model—application to an extreme meteorological event

Since the stage of validation only confirms the model's behaviour under the range of conditions represented by the available data, it was deemed more appropriate to use experimental observations obtained after episodic rainfalls and considerable non-point nutrient fluxes which was the outmost scope for the development of this model. Thus, field data collected from sampling cruises that took place after the occurrence of six storm events, were compared with the respective predicted values. In the present work, both spatial and temporal variations of nutrient and chlorophyll *a* concentrations were deemed as the most appropriate validation criteria to translate the main objectives of the model. The goodness-of-fit between experimental and simulated data was also sought by the two-sided Kolmogorov–Smirnov test (Table 8). It was found that in most cases the simulated values of these variables do not vary significantly from the observed data indicating that the model has a satisfactory ability to predict the dynamics of coastal marine environments under extreme external perturbations such as nutrient enrichment after episodic precipitation events.

This predictive capability of the model enabled the reliable assessment of the contribution of single rainfall events to the dynamics of the gulf. For example, the following results concern the episodic rainfall event (4.75 cm) that took place on the 2nd of April of 1997. The rainfall started on 11.30 a.m. and finished on 9.30 p.m., whereas the prevailing wind during the following three days was characterised by a southeast mean direction and velocities in the range of 3–5 m/s.

The results of the terrestrial submodel are shown in Fig. 6 where the graphs represent the flow rates and the total load of nitrate and phosphate in terms of the time after the rainfall starting. Similar computations were obtained for ammonium and dissolved organic nitrogen. The simulated and experimental data refer to the outlet of the most important torrent of the area,

Table 8
Model validation: results of the two-sided Kolmogorov–Smirnov goodness-of-fit test between experimental and simulated values of the state-variables, after the occurrence of six episodic rainfall events

State variables	Date and total rainfall					
	4/3/1997 (3.81 cm)	2/4/1997 (4.75 cm)	10/12/97 (5.12 cm)	22/12/97 (3.67 cm)	3/2/98 (4.08 cm)	10/3/98 (3.17 cm)
Phytoplanktonic biomass	0.187[a]	0.310[a]	0.354	0.165[a]	0.352	0.241[a]
Nitrate concentration	0.199[a]	0.221[a]	0.362	0.298[a]	0.301[a]	0.227[a]
Ammonium concentration	0.266[a]	0.313[a]	0.180[a]	0.415	0.391	0.424
Phosphate concentration	0.350	0.232[a]	0.426	0.288[a]	0.416	0.322[a]
DOC concentration	0.288[a]	0.154[a]	0.208[a]	0.225[a]	0.259[a]	0.281[a]

[a] Good accordance between simulated and experimental data at the 0.05 level of significance.

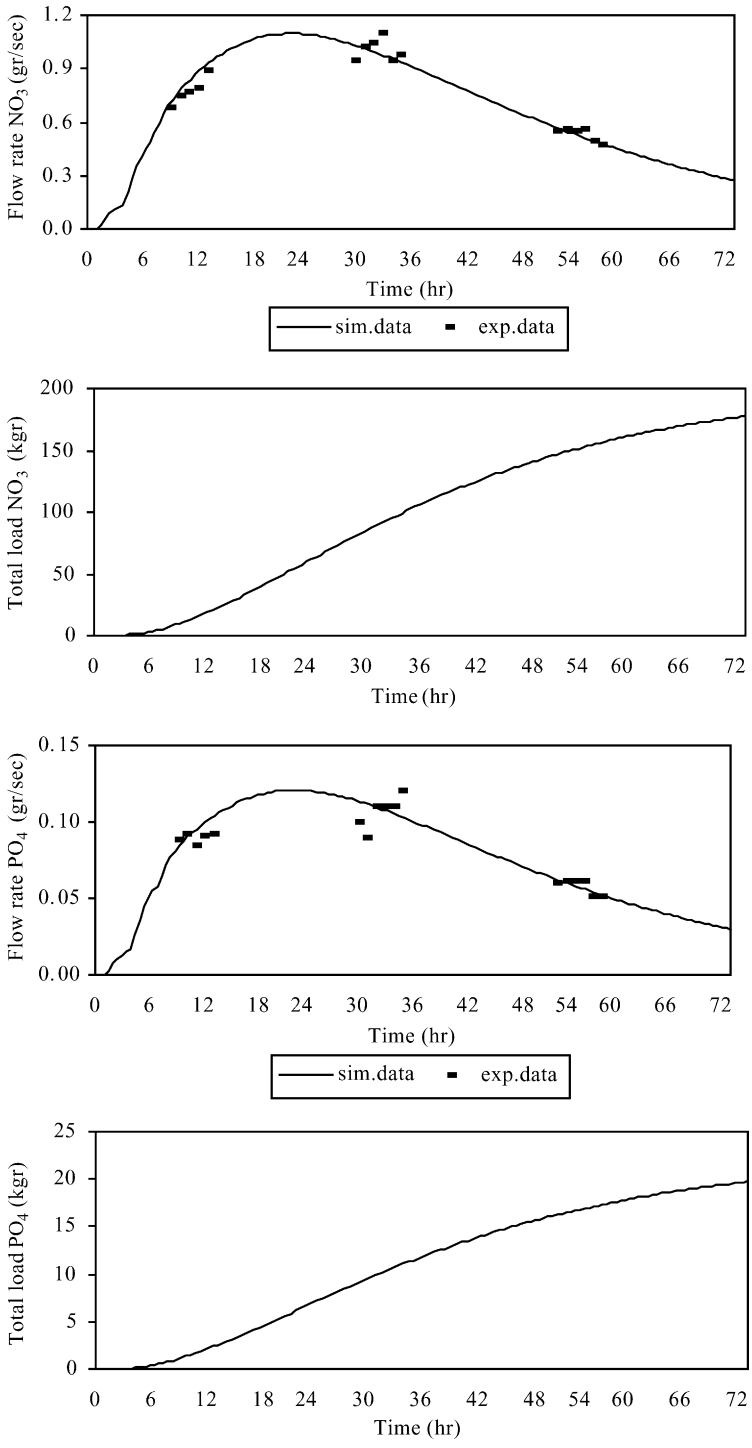

Fig. 6. Flow rate and total load of nitrate and phosphate after an extreme rainfall event (4.75 cm) that took place on 2 April 1997: simulated and experimental data at the outlet of the most important torrent of Gera's watershed.

located in the northern part of the watershed. The peaks of the flow rates were observed 18–30 h after the beginning of the precipitation and the inflows were essential for more than three days. The output of the Princeton Ocean Model, during the period under study, is shown in Fig. 7. It represents the hydrodynamic regime of the area, after the exclusion of tidal motions, forced by the prevailing southeast wind. It is clear that the gulf of Gera was characterised by a cyclonic pattern with current velocities of 0.02–0.03 m/s. Meanwhile, the harmonic analysis indicated that the seawater masses were also governed by a semi-diurnal unequal tide with a mean tidal height of 0.2 m.

The spatial and temporal evolution of nitrate and phosphate concentrations during a period of 3 days after the rainfall event is exposed in the sequences of maps in Figs. 8 and 9. The non-point nitrate fluxes resulted in an increase of the mean concentration of up to 45%, from 0.55 to 0.80 μM. The smaller increase of the phosphates (27%), from 0.55 to 0.70 μM, was due to the smaller dissolved-phase fraction of phosphorus in soil. The most significant inflows took place in the northern and the western part, where the outlets of the two most important torrents of the watershed are located. The subsequent marine areas had higher nutrient concentrations, and in general, the system exposed a spatial heterogeneity during the first 2 days (3–4 April). However, the exogenous loads were dispersed by the tidal and non-tidal transport and it is clear that after the third day (5 April) the system tended to uniformity. The residence time of the excessive nutrients within the gulf is the critical point that determines their availability on the autotrophs; it depends mostly on the exchanges with the open sea. It was computed from the model that this renewal of the seawater ranges from a time span of less than 10 days, as in this particular case, to 1 month period.

Finally, the responses of the primary producers were tested under two alternative scenarios, concerning weather conditions of the following period after the rainfall event (Fig. 10). The first case was that of cloudiness (50% decrease of the I_t value), which in fact corresponded to the real conditions. It resulted in an increase of the chlorophyll a concentration of up to 28%, from 0.7 to 0.9 μg/l, 6 days after the rainfall event. The phytoplankton maxima occurred again in the northwestern part of the gulf, whereas the eastern part presented 0.05–0.1 μg/l lower concentrations. Both spatial and temporal results are in good accordance with the experimental data. On the other hand, the scenario of sunshine was accompanied by a 40% increase of the phytoplanktonic biomass. This output emphasizes the role of the physical forcing, especially of solar radiation, in the equilibrium of this coastal marine ecosystem. It seems that such extreme meteorological events in combination with unfavorable physical conditions (sunshine, large residence time) constitute an indisputable threat for the ecological stability of the gulf.

4.4. Future developments

The present modelling approach has a good fit to the experimental data and describes sufficiently the dynamics of inorganic nutrients–phytoplankton–bacteria-zooplankton and organic carbon relationships. An additional merit is its enhanced spatial resolution and its flexibility in the time discretization. The model provides successful simulations and accounts for both short (h) and long time scales (years). The most significant mechanicistic improvement of the model, though a difficult task, could be the incorporation of the fine particulate matter resulting from soil erosion and sediment perturbation, due to its ambiguous role in the water column (Sharpley et al., 1989).

The modelling of the soil erosion is too difficult due to its complex nature. Many factors and processes influence the hall procedure from its sources until the outlet of the watershed (Hall et al., 1999). Apart from possible measurement errors, these factors include redeposition of sediment in surface water storage, trapping of sediment by vegetation and plant residues and local scour and redeposition in rills and channels (Novotny and Chesters, 1981). Therefore, in the existing literature, we have rough estimators of long-term average erosion and only a small number of event-based loading functions, which are amenable to various uncertainties and assumptions. Similar difficulties are encountered in the modelling of the perturbation, where numerous of processes such as in situ reactions, bulk movements due to wave impingement, density-driven displacement by water of higher salinity and bioturbation regulate the vertical fluxes of particulate matter and the enrichment of the water column (Matisoff and Wang, 1998).

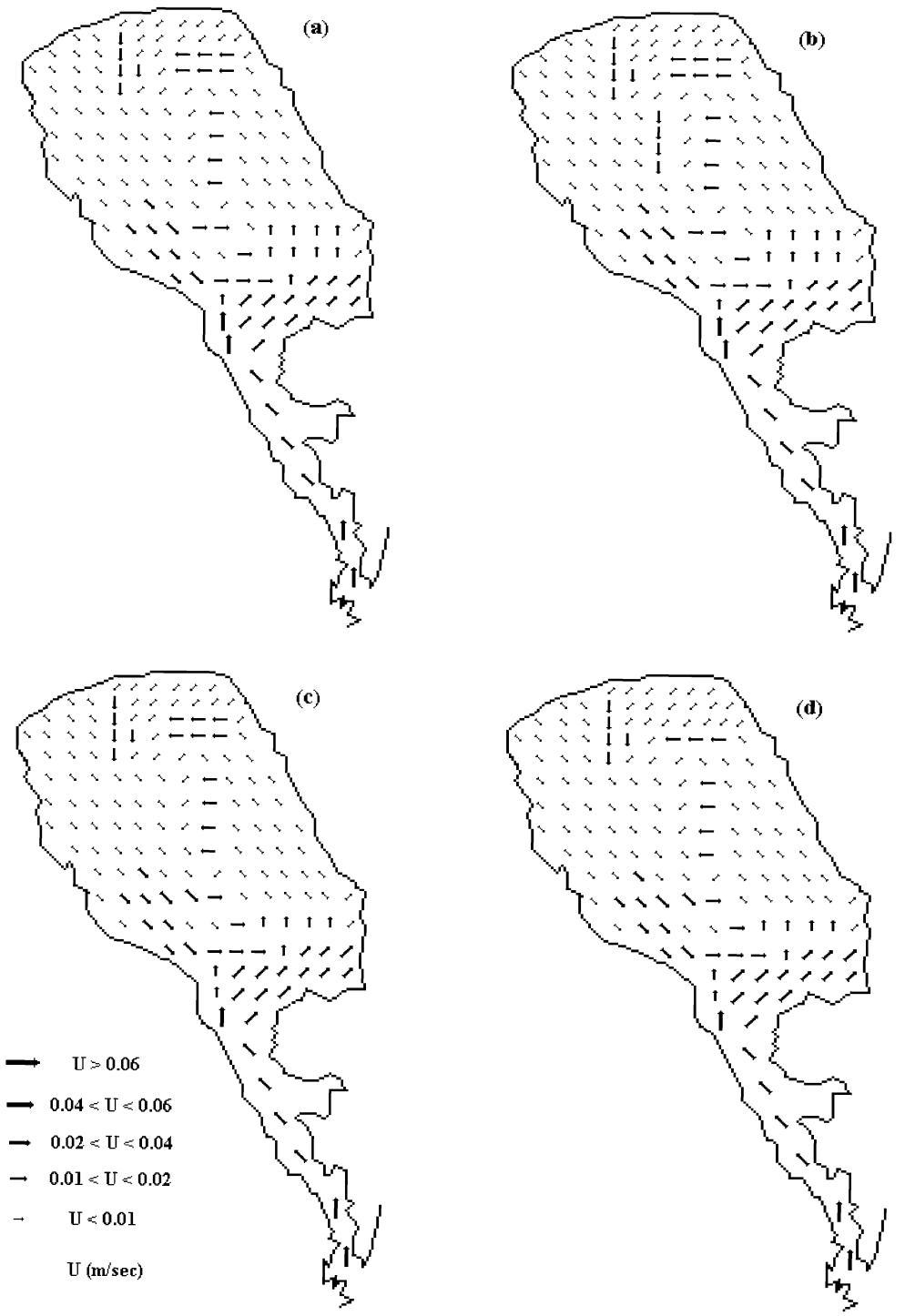

Fig. 7. The circulation pattern of the study area, forced by the prevailing southeast wind pattern, during the period 2–5 April 1997. (Output of the Princeton Ocean Model after the exclusion of the tidal forcing).

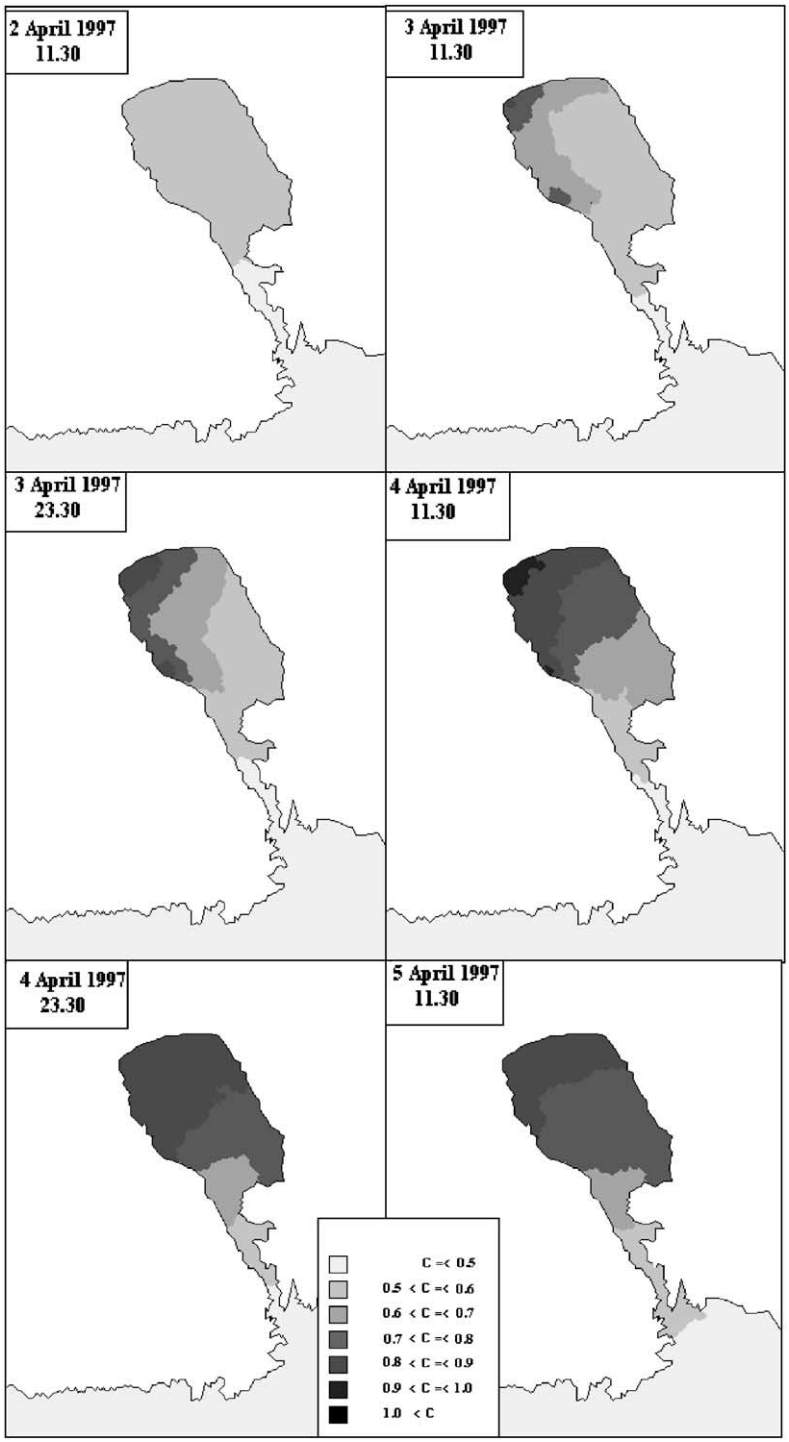

Fig. 8. Temporal and spatial distribution of nitrate (μg-at N/l) in the gulf of Gera, during the period 2–5 April 1997.

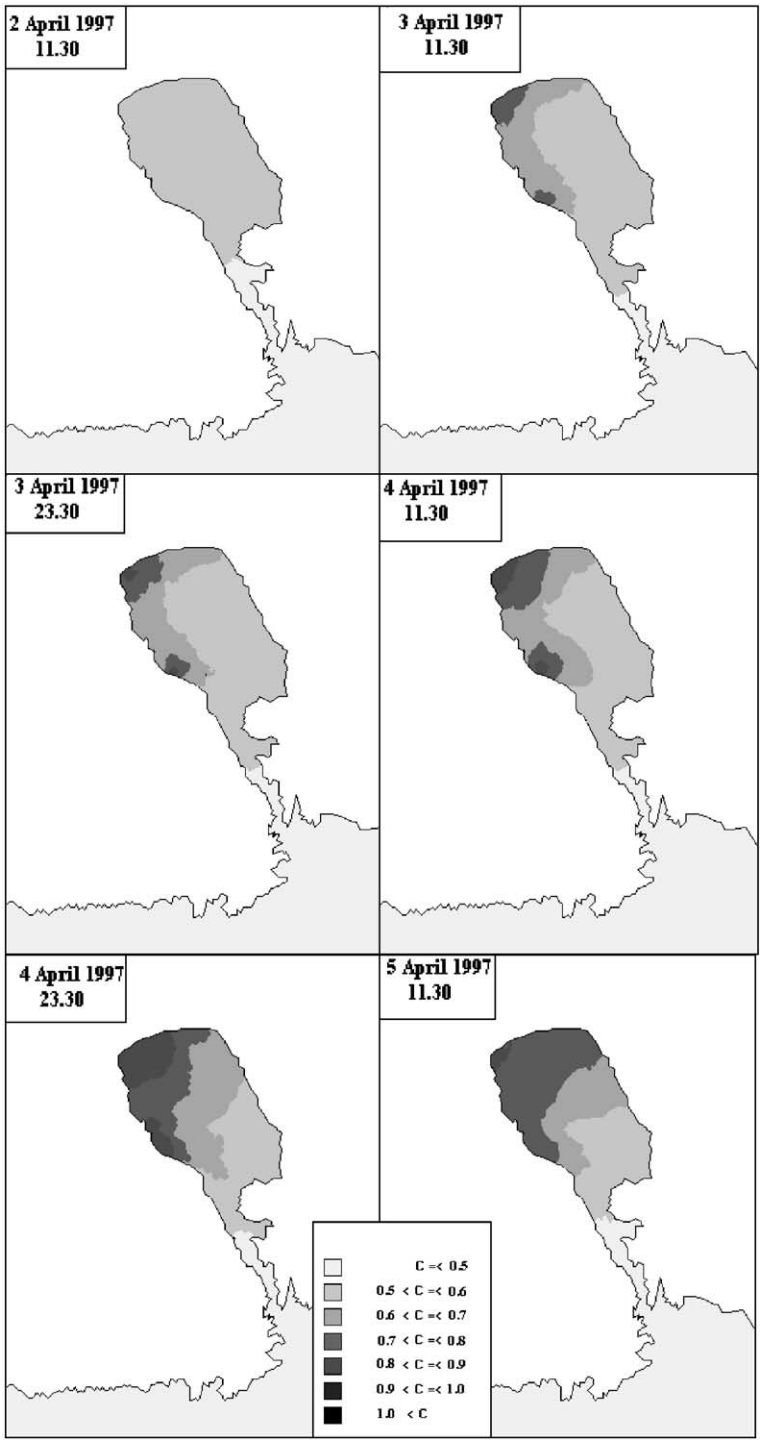

Fig. 9. Temporal and spatial distribution of phosphate (μg-at P/l) in the gulf of Gera, during the period 2–5 April 1997.

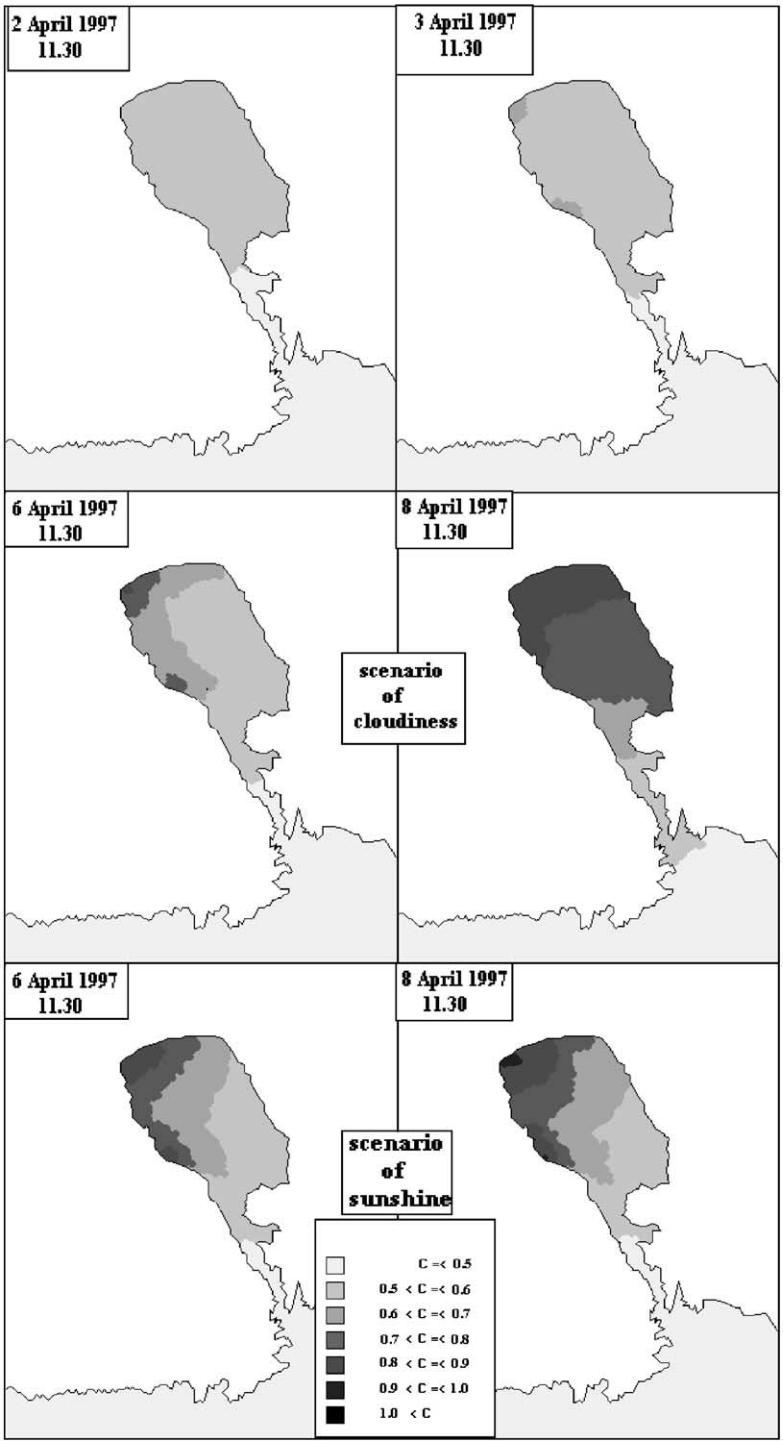

Fig. 10. Temporal and spatial distribution of chlα (μg/l) in the gulf of Gera, during the period 2–8 April 1997, after the scenarios of cloudiness and sunshine.

Sediments transported into the seawater enter a remarkably complicated environment that is also inadequately modelled. They may undergo repeated cycles of erosion, transport and deposition by wave action or ebb-flood tidal currents and be resuspended many times prior to accumulation (Nichols and Boon, 1994). However, some recent trends in ecological modelling should provide useful tools to overcome all these difficulties. The application of expert knowledge, the use of currently changed parameters, the performance of ecological tests to assess the best parameters sets in combination with the presentation of model results as patterns rather than as numerical values are likely to give feasible and workable methodologies that can elucidate the aforementioned intricate processes (Jorgensen, 1997).

References

Arhonditsis, G., 1998. Quantitative assessment of the effects of nonpoint sources to coastal marine eutrophication. PhD Thesis (in Greek, with English abstract), Department of Environmental Studies, University of the Aegean, Mytilene, Greece, 249 pp.

Arhonditsis, G., Tsirtsis, G., Angelidis, G., Karydis, M., 2000a. Quantification of the effects of nonpoint nutrient sources to coastal marine eutrophication: applications to a semi-enclosed gulf in the Meditteranean Sea. Ecological Modelling 129 (2–3), 209–227.

Arhonditsis, G., Giourga, C., Loumou, A., 2000b. Ecological patterns and comparative nutrient dynamics of natural and agricultural Mediterranean-type ecosystems. Environmental Management 26 (5), 527–537.

Arhonditsis, G., Giourga, C., Loumou, A., Koulouri, M., in press. Quantitative assessment of agricultural runoff and soil erosion using mathematical modelling: applications in the Mediterranean region. Environmental Management.

Bouraoui, F., Dillaha, T.A., 1996. Answers-2000: runoff and sediment transport model. Journal of Environmental Engineering 122 (6), 493–502.

Coffaro, G., Bocci, M., 1997. Resources competition between *Ulva rigida* and *Zostera marina*: a quantitative approach applied to the Lagoon of Venice. Ecological Modelling 102, 81–95.

Coffaro, G., Sfriso, A., 1997. Simulation model of *Ulva rigida* growth in shallow water of the Lagoon of Venice. Ecological Modelling 102, 55–66.

Davidson, K., 1996. Modelling microbial food webs. Marine Ecology Progress Series 145, 279–296.

Fasham, M.J.R., Ducklow, H.W., McKelvie, S.M., 1990. A nitrogen-based model of plankton dynamics in the oceanic mixed layer. Journal of Marine Research 48, 591–639.

Hall, R., Leavitt, P.R., Quinlan, R., Dixit, A.S., Smol, J.P., 1999. Effects of agriculture, urbanization and climate on water quality in the northern Great Plains. Limnology and Oceanography 44 (3 part 2), 739–756.

Herut, B., Krom, M., 1996. Atmospheric input of nutrients and dust to the SE Mediterranean. In: Guerzoni, S., Chester, R. (Eds.), The Impact of Desert Dust Across the Mediterranean. Kluwer Academic Publishing, Netherlands, pp. 349–358.

Herut, B., Krom, M., Pan, G., Mortimer, R., 1999. Atmospheric input of nitrogen and phosphorus to the Southeast Mediterranean: sources, fluxes and possible impact. Limnology and Oceanography 44 (7), 1683–1692.

Isaji, T., Spaulding, M.L., Stace, J., 1985. Tidal exchange between a coastal lagoon and offshore waters. Estuaries 8, 203–216.

Jacobsen, O.S., Jorgensen, S.E., 1975. A submodel for nitrogen release from sediments. Ecological Modelling 1, 147–151.

Jorgensen, S.E., 1997. Intergration of Ecosystems Theories: A Pattern, 2nd edn. Kluwer Academic Publishing, Boston, 388 pp.

Kamp-Nielsen, L., 1975. A kinetic approach to the aerobic sediment–water exchange of phosphorus in Lake Esrom. Ecological Modelling 1, 153–160.

Lee, S.H., Fuhrman, J.A., 1987. Relationships between biovolume and biomass of naturally derived marine bacterioplankton. Applied Environmental Microbiology 53, 1298–1303.

Lesack, L.F.W., Marsh, P., Hecky, R.E., 1998. Spatial and temporal dynamics of major solute chemistry among Mackenzie Delta lakes. Limnology and Oceanography 43 (7), 1530–1543.

Marchetti, R., Verna, N., 1992. Quantification of the phosphorus and nitrogen loads in the minor rivers of the Emilia–Romagna coast (Italy). A methodological study on the use of theoretical coefficients in calculating the loads. In: Vollenweider, R.A., Marchetti, R., Viviani, R. (Eds.), Marine Coastal Eutrophication. Elsevier, Amsterdam, pp. 315–335.

Matisoff, G., Wang, X., 1998. Solute transport in sediments by freshwater infaunal bioirrigators. Limnology and Oceanography 43 (7), 1487–1499.

Medinets, V.I., 1996. Shipboard derived concentrations of sulphur and nitrogen compounds and trace metals in the Mediterranean aerosol. In: Guerzoni, S., Chester, R. (Eds.), The Impact of Desert Dust Across the Mediterranean. Kluwer Academic Publishing, Netherlands, pp. 359–368.

Mellor, G.L., 1996. Users Guide for a Three-Dimensional, Primitive Equation, Numerical Ocean Model. Princeton Univ., Princeton, 40 pp.

Mellor, G.L., Yamada, T., 1982. Development of a turbulence closure model for geophysical fluids problems. Reviews of Geophysics 20, 851–875.

Michelakis, N., Koutsaftakis, A., 1989. The Problem with the Wastewater in the Olive Industry. University of Crete, Iraklio, Greece, 190 pp.

Nichols, M.M., Boon, J.D., 1994. Sediment transport processes in coastal lagoons. In: Kjerfve, B. (Ed.), Coastal Lagoon Processes. Elsevier, Amsterdam, pp. 157–209.

Novotny, V., Chesters, G., 1981. Handbook of Nonpoint Pollution: Sources and Management. Van Nostrand Reinhold, New York, 555 pp.

Ozsoy, E., 1977. Flow and mass transport in the vicinity of tidal inlets. Technical Report No. TR-036, Coastal and Oceanographic Engineering Laboratory, University of Florida, Gainesville, FL.

Pond, S., Pickard, G.L., 1983. Introductory Dynamical Oceanography. Pergamon, New York, 329 pp.

Redfield, A.C., Ketcum, B.H., Richards, F.A., 1963. The influence of organisms on the composition of seawater. In: Hill, M.N. (Ed.), The Sea, vol. 2. Interscience, New York, pp. 26–77.

Rinaldo, A., Marani, A., 1987. Basin scale model of solute transport. Water Resources Research 23 (11), 2107–2118.

Shanahan, P., Harleman, D.R.F., 1984. Transport in lake water quality modeling. Journal of Environmental Engineering 110 (1), 42–57.

Sharpley, A.N., Smith, S.J., Menzel, R.G., 1989. Phosphorus dynamics in agricultural runoff and reservoirs in Oklahoma. Lake and Reservoir Management 5 (2), 75–81.

Smith, R.V., 1977. Domestic and agricultural contributions to the inputs of phosphorus and nitrogen to Lough Neagh. Water Research 11, 453–459.

Spaulding, M.L., 1994. Modelling of circulation and dispersion in coastal lagoons. In: Kjerfve, B. (Ed.), Coastal Lagoon Processes. Elsevier, Amsterdam, pp. 103–127.

Steele, J.H., 1962. Environmental control of photosynthesis in the sea. Limnology and Oceanography 7, 137–150.

Taylor, A.H., Joint, I., 1990. A steady-state analysis of the microbial loop in stratified systems. Marine Ecology Progress Series 59, 1–17.

Tsirtsis, G.E., 1995. A simulation model for the description of a eutrophic system with emphasis on the microbial processes. Water Science Technology 32 (9–10), 189–196.

Visser, A.W., Kamp-Nielsen, L., 1996. The use of models in eutrophication studies. In: Jorgensen, B.B., Richardson, K. (Eds.), Coastal and Estuarine Studies. American Geophysical Union, Washington, DC, pp. 221–242.

Watson, D.F., Philip, G.M., 1985. A refinement of inverse distance weighted interpolation. Geo-Processing 2, 315–327.

Weiyan, T., 1992. Shallow Water Hydrodynamics: Mathematical Theory and Numerical Solution of a Two-Dimensional System of Shallow Water Equations. Elsevier, Amsterdam.

Werner, W., Wodsak, H.P., 1994. Germany: the baltic sea and its agricultural environmental status. Marine Pollution Bulletin 29 (6–12), 471–476.

Zingales, F., Marani, A., Rinaldo, A., Bendoricchio, G., 1984. A conceptual model of unit-mass response function for non-point source pollutant runoff. Ecological Modelling 26, 285–311.